Journal of Materials Chemistry A

ROYAL SOCIETY OF CHEMISTRY

COMMUNICATION

View Article Online
View Journal | View Issue

Check for updates

Cite this: J. Mater. Chem. A, 2023, 11, 13209

Received 30th March 2023
Accepted 23rd May 2023

DOI: 10.1039/d3ta01892j

rsc.li/materials-a

Unravelling the CO_2 capture and conversion mechanism of a NiRu–Na_2O switchable dual-function material in various CO_2 utilisation reactions†

Loukia-Pantzechroula Merkouri,[a] Juan Luis Martín-Espejo,[b] Luis F. Bobadilla,[b] José Antonio Odriozola,[b] Anna Penkova,[b] Tomas Ramirez Reina[b] and Melis S. Duyar *[a]

Time-resolved *operando* DRIFTS-MS was performed to elucidate the CO_2 capture and conversion mechanisms of a NiRuNa/CeAl DFM in CO_2 methanation, reverse water–gas shift, and dry reforming of methane. CO_2 was captured mainly in the form of carbonyls and bidentate carbonates, and a spillover mechanism occurred to obtain the desired products.

[a]*School of Chemistry and Chemical Engineering, University of Surrey, Guildford, GU2 7XH, UK. E-mail: m.duyar@surrey.ac.uk*

[b]*Department of Inorganic Chemistry and Materials Sciences Institute, University of Seville-CSIC, 41092, Seville, Spain*

† Electronic supplementary information (ESI) available. See DOI: https://doi.org/10.1039/d3ta01892j

Dr Melis Duyar is a Senior Lecturer in the School of Chemistry and Chemical Engineering at the University of Surrey. She has a research background in heterogeneous catalysis for energy and environmental applications. Her current research interests include the development of novel adsorbent materials for CO_2 capture, catalytic/dual function materials for CO_2 utilisation, and chemical upcycling of microplastics. Dr Duyar received her BSc (2012) in Chemical and Biological Engineering from Koç University. She obtained her M.S. (2013) and PhD (2015) in Earth and Environmental Engineering from Columbia University and conducted post-doctoral research (2015–2017) in the Chemical Engineering Department at Stanford University. Prior to her academic appointment at the University of Surrey (2019), she worked at the US Department of Energy's SLAC National Accelerator Laboratory as Associate Staff Scientist at the SUNCAT Center for Interface Science and Catalysis and was also Lecturer of Chemical Engineering at Stanford University (2017–2019).

Introduction

Efforts to mitigate climate change have recently been intensified as we are approaching 2030, when a significant drop in greenhouse emissions needs to be achieved so as to meet the target of net-zero emissions by 2050.[1–4] Capturing CO_2, either from stationary sources or directly from the air, and storing it in underground formations, or utilising it to produce high-value chemicals and fuels, is considered essential so as to attain the net zero.[5–7] Dual-function materials (DFMs) offer a modular solution to the circular economy since they integrate the CO_2 capture and utilisation steps, eliminating the high costs of CO_2 compression and transportation. Consisting of both a mid-temperature adsorbent and a catalyst, DFMs are able to reversibly capture CO_2 at intermediate temperatures and then convert it into the desired products.[8–10]

The most studied reaction with DFMs is the CO_2 methanation reaction (eqn (1)) and DFMs have been optimised so that CO_2 capture and methanation can be performed at the same temperature, *ca.* 300–350 °C. In addition, the main product is CH_4, or synthetic natural gas, which can be introduced to the current natural gas grid.[11] However, DFMs have been studied in other reactions as well, such as reverse water-gas shift, dry reforming of methane, and dry reforming of ethane, all of which produce syngas with various H_2/CO ratios (eqn (2)–(4)).[12–20] Therefore, it is evident that DFMs can be applicable to a wide range of CO_2 utilisation technologies. Moreover, if the same DFM is able to operate in more than one CO_2 utilisation reaction by simply changing the reaction conditions, it is possible to devise switchable systems that can respond to fluctuations in reactant supply or product demand.[15] By using switchable DFMs, flexible chemical synthesis can be accomplished, thus overcoming the market uncertainties which result from fluctuations in the supply and demand.

$$\text{CO}_2\text{ methanation: } \text{CO}_2 + 4\text{H}_2 \rightarrow \text{CH}_4 + 2\text{H}_2\text{O} \quad (1)$$

$$\text{RWGS: } \text{CO}_2 + \text{H}_2 \rightarrow \text{CO} + \text{H}_2\text{O} \quad (2)$$

Open Access Article. Published on 23 2023. Downloaded on 26.05.2026 23:11:33.
This article is licensed under a Creative Commons Attribution 3.0 Unported Licence.

Open Access Article. Published on 23 2023. Downloaded on 26.05.2026 23:11:33.
This article is licensed under a Creative Commons Attribution 3.0 Unported Licence.

$$\text{DRM: } CO_2 + CH_4 \rightarrow 2CO + 2H_2 \quad (3)$$

$$\text{DER: } 2CO_2 + C_2H_6 \rightarrow 4CO + 3H_2 \quad (4)$$

The urgency of achieving net-zero emissions makes it a priority to understand the DFMs at a fundamental level. By perceiving the various reaction intermediates that are formed and the reaction pathway that each species promotes, connections between structure and activity can be made, leading to a faster DFM optimisation. Diffuse Reflectance Infrared Fourier Transform Spectroscopy (DRIFTS) is a key technique for elucidating the reaction mechanism that is used to observe the evolution of adsorbed, desorbed, and intermediate species over a catalyst surface under working conditions. We have previously shown that NiRuNa/CeAl acts as a switchable DFM that first captures the CO_2 and subsequently catalyses methanation, RWGS, and DRM by adjusting the temperature and co-reactant (H_2 or CH_4) used.[15] We have also demonstrated that CO_2 adsorption on different adsorbent sites also has an effect on selectivity, indicating that the mechanism of reaction on DFMs is closely connected to the interaction of CO_2 with the DFM surface during the capture step, in addition to its interaction with the catalytic sites during the subsequent reduction step. As a result, DRIFTS data can help with the reaction mechanism comprehension in order to synthesise more efficient DFMs in the future, allowing to tune up the selectivity and reactivity of DFMs. Even though some mechanistic studies have been performed for CO_2 capture and utilisation separately,[21–26] there are only few DRIFTS studies of DFMs to date,[12,19,27–30] creating the need for further investigation of the structure–activity relations.

In this project, a DFM consisting of Ni and Ru as the active catalytic species and Na as the adsorbent, prepared and analysed in our previous work,[15] was used to elucidate the mechanism during CO_2 capture and conversion. In particular, 5 cycles of CO_2 capture and conversion were performed, with the targeted reactions being CO_2 methanation, RWGS, and DRM.

Results and discussion

Ex situ characterisation: XPS and particle size analysis

Fig. 1a is a representative TEM image of the NiRuNa sample and Fig. 1b shows its particle size distribution. The average particle size was calculated to be 6.3 nm. Overall, small nanoparticles were observed, showing that a good dispersion of the active species was achieved during the DFM synthesis. XPS results are demonstrated in Fig. 1c and d, displaying the Ru 3p and Na 1s regions. It can be seen that Ru had a mixture of reduced (Ru^0) and oxidised species (Ru^{4+}), with the oxidised species being predominant. This is attributed to the air exposure prior to the measurement of DFM and to the fact that XPS is a surface technique. Previously conducted XRD of the reduced NiRuNa sample showed no Ru^0 peaks despite the fact that the fresh sample displayed RuO_2 peaks, demonstrating the high dispersion of Ru species and/or the Ni–Ru alloy formation,[15] further proving that a thin oxidised layer was formed after air exposure. In Fig. 1d, the Na 1s region presents a single peak at 1071.6 eV ascribed to carbonate species,[31] in accordance with the DRIFTS

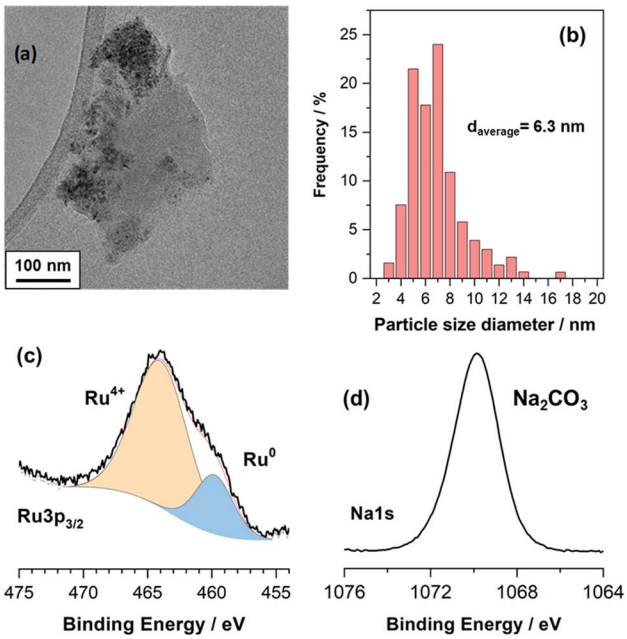

Fig. 1 *Ex situ* characterisation of NiRuNa sample (a) representative TEM image. (b) Particle size distribution based on TEM images. (c) Ru 3p XPS region. (d) Na 1s XPS region.

spectra after reduction (not shown here) and its CO_2-TPD profile showing CO_2 release at room temperature.[15] The Ni and Ce XPS regions can be found in the ESI in Fig. S1.†

Time-resolved *operando* DRIFTS-MS experimental analysis

In order to get insights into the surface intermediates involved and obtain relevant mechanistic aspects during CO_2 capture and subsequent reduction reaction, we performed an *operando* DRIFTS-MS study by alternating successive CO_2 capture and H_2 or CH_4 cycles under isothermal conditions at 250 °C for methanation and 550 °C for RWGS and DRM reactions. MS-data can be found in the ESI in Fig. S2, S3, and S4.†

CO_2 capture and methanation

Fig. 2a contains a bidimensional representation of the dynamic evolution of the spectra successively recorded during the alternated cycles of CO_2 capture and methanation at 250 °C. All IR spectra were subtracted with respect to the spectrum of the surface activation for distinguishing between emerging and disappearing species. As can be noticed, the development of bands ascribed to gaseous CO_2 (2360 cm^{-1}) and the symmetric/asymmetric stretching OCO vibrations typical of carbonate species (1600–1300 cm^{-1}) were clearly distinguished during the CO_2 capture period. It is also worth observing the appearance of bands ascribed to CO adsorbed on metal sites (1900–2000 cm^{-1}) during the capture step, revealing that CO_2 may be dissociatively adsorbed as CO* and O* species. The presence of ruthenium decreased the energy barrier for CO_2 dissociation and promoted the subsequent hydrogenation of CO* adsorbed species.[32] Likewise, CO_2 could also be reduced to CO onto the oxygen-deficient sites of the CeO_2–Al_2O_3 support, and CO

 This journal is © The Royal Society of Chemistry 2023

Open Access Article. Published on 23 2023. Downloaded on 26.05.2026 23:11:33.
This article is licensed under a Creative Commons Attribution 3.0 Unported Licence.

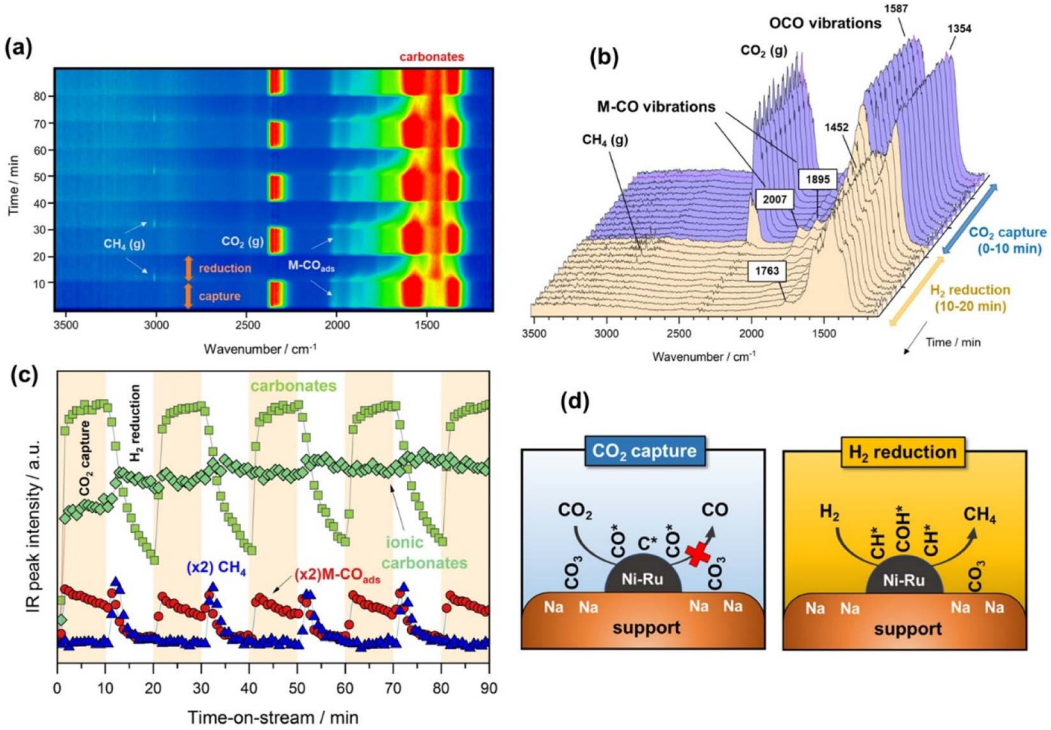

Fig. 2 (a) Bidimensional representation of time-resolved DRIFTS spectra on the reduced NiRuNa/CeAl during capture/reduction cycles (10% CO_2 in Ar and 10% H_2 in Ar, both at 50 mL min^{-1}) at 250 °C. (b) Representative evolution of spectra during the first cycle of capture/reduction. (c) Evolution of selected IR bands signal during the capture/reduction cycles: CH_4 (3016 cm^{-1}), ionic carbonates (1452 cm^{-1}), carbonates (1587 cm^{-1}) and M–CO_{ads} (2007 cm^{-1}) (d) illustrative sketch of the capture/reduction process on NiRuNa/CeAl.

migrated to form carbonyl species adsorbed on metal sites.[33] This was coherent with the absence of gaseous CO. After switching from the CO_2 capture to H_2 reduction stream, the evolution of a new band at 3016 cm^{-1} attributed to gaseous methane was observed, which was the predominant product.

In more detail, Fig. 2b shows the evolution of the IR spectra collected during the first cycle of capture/reduction. As can be seen, the spectra recorded during the CO_2 capture stage (0–10 min) were dominated by the presence of two intense bands in the 1800–1200 cm^{-1} region. These bands were ascribed to the symmetric and asymmetric stretching vibrations related to carbonate-like species with different adsorption geometry on the basic sites of the support. Accordingly, the pair of bands at 1587–1354 cm^{-1} ($\Delta\nu_3$ splitting = 233) were associated with bridged or bidentate carbonates.[28,34,35] It has been suggested that CO_2 is preferably adsorbed, forming bidentate carbonates on Al–O–Na sites over Na-promoted catalysts.[28] It is noteworthy that the intensity of these bands only decreased slightly after switching to the 10% H_2/Ar stream, indicating that bidentate carbonates were only partially removed at 250 °C. In addition, other two features at 1452 and 1763 cm^{-1} were clearly visible and remained stable during the reduction step. These two bands are typical of very symmetric D_{3h} alkali carbonates with high ionicity degree.[36,37] As can be observed, these species were highly stable and remained on the surface upon switching to the reduction stream. Moreover, it should be noted that bicarbonate species could be formed by reaction between CO_2 and surface hydroxyls. However, the bands related to bicarbonate species (1225, 1430, and 1650 cm^{-1}) were absent due to the fact that sodium addition neutralised the hydroxyl groups on the support surface.[38]

As regards the bands developed in the CO stretching region (2100–1800 cm^{-1}), two bands at 2007 and 1895 cm^{-1} emerged during the capture step. These two features were respectively ascribed to linear and bridged carbonyl-adsorbed species on metallic sites. In our recent work,[39] we suggested that an induced electron transfer from Ru to Ni atoms, resulting in metallic sites with high electron density existed, redshifting the carbonyl stretching vibrations. The presence of carbonyl-adsorbed species during CO_2 capture step revealed that CO_2 was partially dissociated into CO* and O* on metallic sites, or reduced on the oxygen vacancies of the cerium-promoted sites of the support. Besides, the fact that CO was further dissociated into C* and O* species could not be ruled out in this case because it is known that this path is facilitated by Ru sites.[40] It should be noted that vibrational modes of carbon species are hardly detectable by IR.

Fig. 2c displays the evolution of the IR bands intensities ascribed to bidentate carbonates (1587 cm^{-1}), ionic carbonates (1452 cm^{-1}), linearly CO* bounded species (2007 cm^{-1}), and CH_4 gas formation (3016 cm^{-1}) as a function of time during the successive capture and reduction cycles. It is interesting to note that upon switching to the H_2 stream, bidentate carbonates were partially depleted with a simultaneous increase in the

Open Access Article. Published on 23 2023. Downloaded on 26.05.2026 23:11:33.
This article is licensed under a Creative Commons Attribution 3.0 Unported Licence.

concentration M–CO adsorbed species and production of methane. Likewise, it was clearly evidenced that ionic carbonates were accumulated on the surface. These species were thermally stable and required higher temperatures to be decomposed and/or reduced. Based on these observations, we could conclude that bidentate carbonates were reduced to CO* adsorbed species and subsequently hydrogenated into methane in a sequential reaction pathway (eqn (5)).

$$CO_2 \rightarrow CO_3^{=} \rightarrow CO^* \rightarrow CHO^* \rightarrow CH_x^* \rightarrow CH_4 \quad (5)$$

Loveless *et al.*[41] report that the step of CO hydrogenation on ruthenium sites involves the formation of formyl species (CHO*) that are subsequently hydrogenated into methane or larger hydrocarbons. In another theoretical study, in which density functional theory (DFT) calculations were applied, it was calculated that the direct dissociation of CO_2 to CO* and O* is favoured on Ru (0001) terraces, and that the subsequent CO hydrogenation occurs *via* either COH* or CHO* intermediates formation.[32] Although formyl species were scarcely detected in our study, we could not overlook their presence in the form of very kinetically labile intermediates. Accordingly, Fig. 2d includes a schematic representation of the steps involved in the CO_2 capture and H_2 reduction steps.

CO_2 capture and reverse water–gas shift

In the following case study, analogous successive cycles of CO_2 capture and H_2 reduction were performed at 500 °C to enable the RWGS against the methanation reaction. As can be observed in Fig. 3a and b, the bands involved in the process at 500 °C were similar to those observed at 250 °C. However, it was remarkable that upon switching to H_2 atmosphere, most of the captured CO_2 like bidentate (1587–1354 cm^{-1}) and ionic carbonate (1452 cm^{-1}) species reacted with H_2 over the NiRu active sites, releasing the reduction product composed predominantly by gaseous CO accompanied by some traces of CH_4. The IR intensity profiles shown in Fig. 3c clearly evidence that the reduction kinetic of carbonates was much faster at 500 °C, and the surface was regenerated to initiate a new cycle of capture after reduction. As can be noticed, the formation of carbonates during CO_2 capture step was accompanied by dissociation of CO_2, which was more facile at 500 °C, achieving high initial coverage of CO* adsorbed species (linear at 2007 cm^{-1} and bridged at 1895 cm^{-1}), which were in turn progressively desorbed, releasing CO gas. As sketched in Fig. 3d, we propose two parallel routes for CO formation during integrated CO_2 capture and RWGS. The first route is an associative reaction mechanism in which carbonates species are formed during CO_2 capture phase and subsequently reduced to CO gas during the reduction stage. At the same time, a dissociative mechanism also occurs on the metal sites during CO_2 capture step in which CO* adsorbed species (linear and bridged) are formed and subsequently desorbed, liberating CO gas (Fig. S3†). Accordingly, Fig. 3c and S3† show that CO gas was released in two routes, evident from the two peaks ascribed to the adsorbed CO* species on the metal sites and the CO gas from the

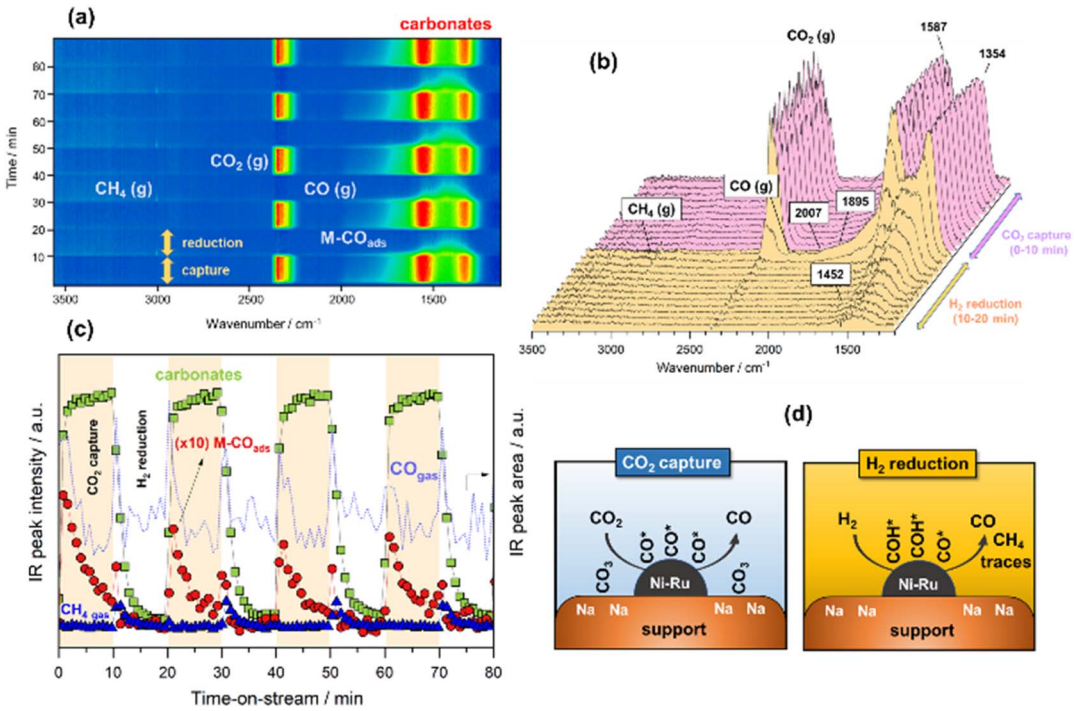

Fig. 3 (a) Bidimensional representation of time-resolved DRIFTS spectra on the reduced NiRuNa/CeAl during capture/reduction cycles (10% CO_2 in Ar and 10% H_2 in Ar, both at 50 mL min^{-1}) at 500 °C. (b) Representative evolution of spectra during the first cycle of capture/reduction. (c) Evolution of selected IR bands signal during the capture/reduction cycles: CO gas (area of left-peak at 2143 cm^{-1}), carbonates (1587 cm^{-1}) and M–CO_{ads} (2007 cm^{-1}) (d) illustrative sketch of the capture/reduction process on NRuNa/CeAl.

 This journal is © The Royal Society of Chemistry 2023

Open Access Article. Published on 23 2023. Downloaded on 26.05.2026 23:11:33.
This article is licensed under a Creative Commons Attribution 3.0 Unported Licence.

reduction of carbonates. The presence of some traces of methane could be explained, considering that the temperature was not sufficiently high from the thermodynamic viewpoint so as to completely favour the RWGS reaction against methanation, and minor quantities of CO* adsorbed species and/or carbonates were sequentially reduced to methane.

Some authors have proposed that the reduction of CO_2 either to methane or CO takes place *via* the formation of formates following an associative mechanism. For instance, Proaño *et al.*[27] suggest that methanation occurs through sequential hydrogenation with formates as reaction intermediaries. It is well known that bicarbonates are firstly formed by the reaction of CO_2 with hydroxyls, and they are subsequently reduced to formates at the metal/support interfacial sites. The formates are the main intermediates for producing CO or CH_4 depending on the reaction conditions.[26] In our study, we observed that the reaction followed a different reaction pathway since the hydroxyls were neutralised with sodium, and the formation of bicarbonates was inhibited. Consequently, formates could not be produced. Herein, the initial step involved the reduction of carbonates to CO* adsorbed species and the subsequent formation of HCO* intermediates by hydrogenation of CO* adsorbed species onto the metal sites. In the case of methanation, the following step comprised the reaction between HCO* and H* to form HCOH* species, which dissociated into CH* and OH* with the subsequent hydrogenation into methane.[41] In the case of RWGS, the hydrogenation of CO* was inhibited by the temperature, and CO was directly released. A similar mechanism was proposed by Hu and Urakawa,[19] who found that alkali promoted catalysts lead to the formation of formyls and bidentate carbonates as main intermediates for the methanation reaction, but with the formyl species being the most active surface species for the CH_4 production.

CO_2 capture and dry reforming of methane

Finally, in the last approach unsteady-state, dry reforming reaction was performed by alternatingly passing 10% CO_2/Ar and 10% CH_4/Ar gas streams under isothermal conditions at 500 °C. It should be stressed that this approach made use of the coke generated by methane dissociation to reduce the CO_2 captured, following a process known as chemical looping CH_4 conversion coupled with CO_2 utilisation.[42] In our case study, the cycles started by the CH_4 reduction atmosphere and successive cycles of reduction/capture were performed. As shown in Fig. 4a, several weak features emerged in the 1700–1300 and 3300–3100 cm^{-1} regions when the flow of 10% CH_4/Ar was introduced. The intensity of these bands became gradually more intense when the CH_4 exposure was advancing during the cycles. More specifically, two bands at 1340 and 1663 cm^{-1} (Fig. 4b) together with another broad one centred at 3245 cm^{-1} (shown in Fig. 4a) were ascribed to vibrational modes characteristic of graphitic carbon,[43] which was produced from the CH_4 decomposition favoured at this low reforming temperature by thermodynamics.[44] More specifically, the bands at 1663 and 1340 cm^{-1} were respectively ascribed to conjugated C=C stretching vibrations and cyclic carbon groups, whereas the band at 3245 cm^{-1} may have been related to "in-plane" overtones of highly ordered or crystalline graphite.[45–48] This reaction was confirmed by the simultaneous production of H_2, detected by MS (Fig. S4†). On the other hand, it was observed from Fig. 4b that bands, typical of bidentate carbonates (1587–1354 cm^{-1}), were formed during the CO_2 capture phase with simultaneous production of CO gas. In addition, the presence of CO* adsorbed species with linear (2007 cm^{-1}) and bridged (1895 cm^{-1}) coordination on metal sites was detected, while it was also possible that Ru could have further promoted CO* dissociation into C* and O*, as mentioned earlier. It should be remarked that in this case, the CO production was not only attributed to the CO_2 dissociation on metal active sites, but also to the gasification of the C^*/CH_x^* species, following the reverse Boudouard reaction shown below (eqn (6)).

$$CO_2 + C^* \leftrightharpoons CO \quad (6)$$

This fact was reflected in Fig. 4c, where the first cycle of CO_2 capture clearly showed two differentiated peaks of CO production, both related to CO_2 dissociation and CO_2 gasification. It should be noted that the first peak of the CO progressively dropped, whereas the second one dropped more drastically. At the same time, the intensity of the band at 3245 cm^{-1} ascribed to highly ordered graphitic carbon increased with the time of reaction regardless of the gas used, *i.e.* CO_2 or CH_4. This implied slower kinetics of the coke gasification by CO_2 during the capture step than the kinetics of the overall coke formation and consequently, a rapid deactivation of the catalyst in which the nickel metal sites became blocked and the support's pores were recovered with carbonaceous deposits. Fig. 4d includes a representative illustration of the phenomena occurring in both the CH_4 reduction and CO_2 capture steps. Coke is hardly avoided under these conditions due to the thermodynamic restrictions as mentioned earlier, and its accumulation on the catalyst surface causes deactivation. However, this culprit can be overcome using temperatures above 700 °C, in which the endothermic Boudouard reaction is thermodynamically and kinetically more favoured.

It is worth mentioning that these DRIFTS findings were in contrast to our previous work, demonstrating that when the DFM was exposed to CO_2 and then CH_4, the captured CO_2 was converted into CO.[15] Consequently, the order of gases, CH_4 and CO_2, affected the performance of the material. DRIFTS indicated that CO_2 was adsorbed onto the adsorbent sites (carbonates signal), but only part of this signal disappeared upon re-exposure to CH_4. In contrast to our previous findings,[15] upon exposure to CH_4, the adsorbed CO_2 was partially released as CO_2 (gas peak shown in Fig. 4a), and the rest remained adsorbed as carbonates, meaning that none was converted into CO during the DRM step, as the MS data in Fig. S4† and the CO gas signal in Fig. 4c confirmed. When comparing the DRIFTS data for DRM and RWGS, it was observed that in the RWGS experiments almost all the carbonate peaks disappeared upon

Open Access Article. Published on 23 2023. Downloaded on 26.05.2026 23:11:33.
This article is licensed under a Creative Commons Attribution 3.0 Unported Licence.

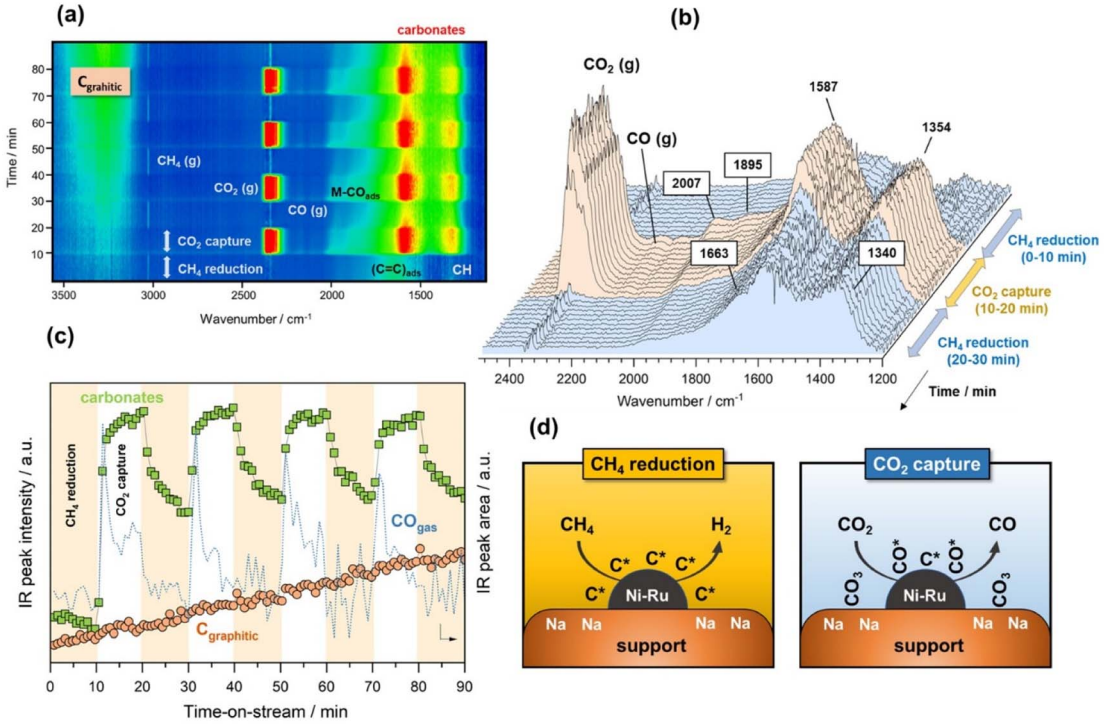

Fig. 4 (a) Bidimensional representation of time-resolved DRIFTS spectra on the reduced NiRuNa/CeAl during reduction/capture cycles (10% CH_4 in Ar and 10% CO_2 in Ar, both at 50 mL min^{-1}) at 500 °C. (b) Representative evolution of spectra during the first cycle of reduction/capture/reduction. (c) Evolution of selected IR bands signal during the capture/reduction cycles: CO gas (area of left-peak at 2143 cm^{-1}), carbonates (1587 cm^{-1}) and $=CH_{ads}$ (3245 cm^{-1}) (d) illustrative sketch of the capture/reduction process on NiRuNa/CeAl.

exposure to H_2. An explanation for that might be that not all the CO_2 was captured reversibly and that some of the carbonates formed at a Na–Ni/Ru interface. If that interface was coke free, it would have allowed further conversion into CO. By performing CH_4 cracking first, these metal/adsorbent interfaces were blocked, preventing the captured CO_2 from reacting. This mechanism highlights the need to control methane cracking during DRM operation of the DFM, through process engineering and material design.

Conclusions

Time-resolved *operando* DRIFTS was performed to understand the mechanism of CO_2 capture and then, CO_2 methanation, RWGS, or DRM on a NiRuNa/CeAl DFM. This was the first mechanistic study on a switchable DFM, providing us with insight into three important CO_2 utilisation reaction pathways that were previously unknown. In this work, it was revealed that during the capture step, CO_2 was dissociated on the metallic sites and reduced on the oxygen-deficient sites of Ce, and that bridged and bidentate carbonates were also formed. During the DRM capture step, CO was also produced due to the coke gasification with the available CO_2, while CH_4 decomposition took place during the DRM step, producing H_2. As far as the conversion steps are concerned, the formation of HCO* intermediates by hydrogenation of CO* adsorbed species onto the metal sites was observed when H_2 was used as a co-reactant. However, CO was liberated in the case of RWGS, while it was subsequently hydrogenated into CH_4 in the case of CO_2 methanation. Overall, it was evident that these findings elucidated the reaction mechanism of DFMs, paving the way of optimised materials formulations in the near future, with maximised catalyst–adsorbent interface, tuned adsorption strength, and site distribution so as to achieve full conversion and higher selectivity.

Author contributions

Loukia-Pantzechroula Merkouri: conceptualisation, methodology, validation, formal analysis, investigation, writing – original draft, visualisation. Juan Luis Martín-Espejo: methodology, validation, formal analysis, investigation, visualisation. Luis Francisco Bobadilla: methodology, formal analysis, resources, writing – original draft, writing – review & editing, visualisation, supervision. José Antonio Odriozola: formal analysis, resources, funding acquisition. Anna Penkova: formal analysis, investigation. Tomás Ramirez Reina: conceptualisation, methodology, resources, writing – review & editing, supervision, project administration, funding acquisition. Melis S. Duyar: conceptualisation, methodology, resources, writing – review & editing, supervision, project administration, funding acquisition.

Conflicts of interest

There are no conflicts to declare.

This journal is © The Royal Society of Chemistry 2023

Open Access Article. Published on 23 2023. Downloaded on 26.05.2026 23:11:33.
This article is licensed under a Creative Commons Attribution 3.0 Unported Licence.

Acknowledgements

This research was funded by the School of Chemistry and Chemical Engineering and the Doctoral College of the University of Surrey. This work was partially sponsored by the European Commission through the H2020-MSCA-RISE-2020 BIOALL project (Grant Agreement: 101008058). L. P. Merkouri acknowledges the Erasmus+ programme, which allowed her to conduct part of the experiments in Seville, Spain. L.-P. Merkouri also thanks Dr Vlad Stolojan of the Department of Electrical and Electronic Engineering for his assistance with TEM training. The team at University of Seville also acknowledge financial support from the Spanish Ministry of Science through the projects NICER-BIOFUELS (ref: PLEC2021-008086), sponsored by MCIN/AEI/10.13039/501100011033 Next Generation Europe SMART-FTS (ref: PID2021-126876OB-I00).

Notes and references

1 United Nations Framework Convention on Climate Change, *Adoption of the Paris Agreement*, Paris, 2015.
2 J. Rogelj, M. Den Elzen, N. Höhne, T. Fransen, H. Fekete, H. Winkler, R. Schaeffer, F. Sha, K. Riahi and M. Meinshausen, *Nature*, 2016, **534**, 631–639.
3 United Nations, *Climate change: No 'credible pathway' to 1.5C limit*, UNEP warns, accessed 3 March 2023, **https://news.un.org/en/story/2022/10/1129912**.
4 IEA, *An updated roadmap to Net Zero Emissions by 2050*, accessed 9 December 2022, **https://www.iea.org/reports/world-energy-outlook-2022/an-updated-roadmap-to-net-zero-emissions-by-2050**.
5 IEA, *CCUS in the transition to net-zero emissions*, accessed 3 March 2023, **https://www.iea.org/reports/ccus-in-clean-energy-transitions/ccus-in-the-transition-to-net-zero-emissions**.
6 J. C. M. Pires, F. G. Martins, M. C. M. Alvim-Ferraz and M. Simões, *Chem. Eng. Res. Des.*, 2011, **89**, 1446–1460.
7 A. Al-Mamoori, A. Krishnamurthy, A. A. Rownaghi and F. Rezaei, *Energy Technol.*, 2017, **5**, 834–849.
8 L. P. Merkouri, T. R. Reina and M. S. Duyar, *Energy Fuels*, 2021, **35**, 19859–19880.
9 I. S. Omodolor, H. O. Otor, J. A. Andonegui, B. J. Allen and A. C. Alba-Rubio, *Ind. Eng. Chem. Res.*, 2020, **59**, 17612–17631.
10 S. Sun, H. Sun, P. T. Williams and C. Wu, *Sustainable Energy Fuels*, 2021, **5**, 4546–4559.
11 M. S. Duyar, M. A. A. Treviño and R. J. Farrauto, *Appl. Catal., B*, 2015, **168–169**, 370–376.
12 H. Sun, J. Wang, J. Zhao, B. Shen, J. Shi, J. Huang and C. Wu, *Appl. Catal., B*, 2019, **244**, 63–75.
13 H. Sun, Y. Wang, S. Xu, A. I. Osman, G. Stenning, J. Han, S. Sun, D. Rooney, P. T. Williams, F. Wang and C. Wu, *Fuel*, 2021, **286**, 119308.
14 A. Al-Mamoori, A. A. Rownaghi and F. Rezaei, *ACS Sustainable Chem. Eng.*, 2018, **6**, 13551–13561.
15 L.-P. Merkouri, R. Reina and M. S. Duyar, *Nanoscale*, 2022, **14**, 12620–12637.
16 S. Bin Jo, J. H. Woo, J. H. Lee, T. Y. Kim, H. I. Kang, S. C. Lee and J. C. Kim, *Sustainable Energy Fuels*, 2020, **4**, 5543–5549.
17 S. Jo, J. H. Lee, J. H. Woo, T.-Y. Kim, H.-J. Ryu, B. Hwang, J. C. Kim, S. C. Lee and K. L. Gilliard-AbdulAziz, *Sustainable Energy Fuels*, 2022, **6**, 81–88.
18 L. F. Bobadilla, J. M. Riesco-García, G. Penelás-Pérez and A. Urakawa, *J. CO_2 Util.*, 2016, **14**, 106–111.
19 L. Hu and A. Urakawa, *J. CO_2 Util.*, 2018, **25**, 323–329.
20 S. Sun, Z. Lv, Y. Qiao, C. Qin, S. Xu and C. Wu, *Carbon Capture Sci. Technol.*, 2021, **1**, 100001.
21 J. Graciani, K. Mudiyanselage, F. Xu, A. E. Baber, J. Evans, S. D. Senanayake, D. J. Stacchiola, P. Liu, J. Hrbek, J. F. Sanz and J. A. Rodriguez, *Science*, 2014, **345**, 546–550.
22 S. C. Qi, J. K. Wu, J. Lu, G. X. Yu, R. R. Zhu, Y. Liu, X. Q. Liu and L. B. Sun, *J. Mater. Chem. A*, 2019, **7**, 17842–17853.
23 S. C. Qi, X. Y. Liu, R. R. Zhu, D. M. Xue, X. Q. Liu and L. B. Sun, *Chem. Eng. J.*, 2022, **430**, 132784.
24 C. Vogt, J. Kranenborg, M. Monai and B. M. Weckhuysen, *ACS Catal.*, 2020, **10**, 1428–1438.
25 M. T. Dunstan, F. Donat, A. H. Bork, C. P. Grey and C. R. Müller, *Chem. Rev.*, 2021, **121**, 12681–12745.
26 X. Wang, Y. Hong, H. Shi and J. Szanyi, *J. Catal.*, 2016, **343**, 185–195.
27 L. Proaño, E. Tello, M. A. Arellano-Trevino, S. Wang, R. J. Farrauto and M. Cobo, *Appl. Surf. Sci.*, 2019, **479**, 25–30.
28 L. Proaño, M. A. Arellano-Treviño, R. J. Farrauto, M. Figueredo, C. Jeong-Potter and M. Cobo, *Appl. Surf. Sci.*, 2020, **533**, 147469.
29 D. Pinto, V. Van der Bom Estadella and A. Urakawa, *Catal. Sci. Technol.*, 2022, **12**, 5349–5359.
30 Z. Zhou, N. Sun, B. Wang, Z. Han, S. Cao, D. Hu, T. Zhu, Q. Shen and W. Wei, *ChemSusChem*, 2020, **13**, 360–368.
31 J. F. Moulder, W. F. Stickle, P. E. Sobol and K. D. Bomben, *Handbook of X-Ray Photoelectron Spectroscopy*, 1979, vol. 3.
32 S. T. Zhang, H. Yan, M. Wei, D. G. Evans and X. Duan, *RSC Adv.*, 2014, **4**, 30241–30249.
33 M. Zhu, P. Tian, X. Cao, J. Chen, T. Pu, B. Shi, J. Xu, J. Moon, Z. Wu and Y. F. Han, *Appl. Catal., B*, 2021, **282**, 119561.
34 L. Azancot, L. F. Bobadilla, M. A. Centeno and J. A. Odriozola, *Appl. Catal., B*, 2021, **285**, 119822.
35 G. Busca and V. Lorenzelli, *Mater. Chem.*, 1982, **7**, 89–126.
36 S. Joshi, S. Kalyanasundaram and V. Balasubramanian, *Appl. Spectrosc.*, 2013, **67**, 841–845.
37 J. Kiefer, A. Strk, A. L. Kiefer and H. Glade, *Energies*, 2018, **11**, 798.
38 S. Navarro-Jaén, A. Szego, L. F. Bobadilla, Ó. H. Laguna, F. Romero-Sarria, M. A. Centeno and J. A. Odriozola, *ChemCatChem*, 2019, **11**, 2063–2068.
39 L. Merkouri, J. L. Martín-espejo, L. F. Bobadilla, J. A. Odriozola, M. S. Duyar and T. R. Reina, *Nanomaterials*, 2023, **13**, 506.
40 J. Wang, Y. Wang and K. Jacobi, *Surf. Sci.*, 2001, **488**, 83–89.
41 B. T. Loveless, C. Buda, M. Neurock and E. Iglesia, *J. Am. Chem. Soc.*, 2013, **135**, 6107–6121.
42 Z. Zhou, Z. Sun and L. Duan, *Curr. Opin. Green Sustainable Chem.*, 2023, **39**, 100721.

43 V. Ţucureanu, A. Matei and A. M. Avram, *Crit. Rev. Anal. Chem.*, 2016, **46**, 502–520.
44 T. Stroud, T. J. Smith, E. Le Saché, J. L. Santos, M. A. Centeno, H. Arellano-Garcia, J. A. Odriozola and T. R. Reina, *Appl. Catal., B*, 2018, **224**, 125–135.
45 L. Bokobza, J. L. Bruneel and M. Couzi, *Vib. Spectrosc.*, 2014, **74**, 57–63.
46 B. Manoj, A. M. Raj and G. C. Thomas, *Sci. Rep.*, 2018, **8**, 13891.
47 R. J. Nemanich and S. A. Solin, *Phys. Rev.*, 1979, **20**, 392–401.
48 Y. Wang, D. C. Alsmeyer and R. L. McCreery, *Chem. Mater.*, 1990, **2**, 557–563.

Open Access Article. Published on 23 2023. Downloaded on 26.05.2026 23:11:33.
This article is licensed under a Creative Commons Attribution 3.0 Unported Licence.

This journal is © The Royal Society of Chemistry 2023